Origin of the phase transition in $IrTe_2$: Structural modulation and local bonding instability

Huibo Cao,[1,*] Bryan C. Chakoumakos,[1] Xin Chen,[2] Jiaqiang Yan,[2,3] Michael A. McGuire,[2] Hui Yang,[3,4] Radu Custelcean,[5] Haidong Zhou,[6,7] David J. Singh,[2] and David Mandrus[2,3]

[1]*Quantum Condensed Matter Division, Oak Ridge National Laboratory, Oak Ridge, Tennessee 37831, USA*
[2]*Materials Science and Technology Division, Oak Ridge National Laboratory, Oak Ridge, Tennessee 37831, USA*
[3]*Department of Materials Science and Engineering, University of Tennessee, Knoxville, Tennessee 37996, USA*
[4]*Institute of Materials and Metallurgy, Northeastern University, Shenyang 110004, People's Republic of China*
[5]*Chemical Sciences Division, Oak Ridge National Laboratory, Oak Ridge, Tennessee 37831, USA*
[6]*Department of Physics and Astronomy, University of Tennessee, Knoxville, Tennessee 37996-1200, USA*
[7]*National High Magnetic Field Laboratory, Florida State University, Tallahassee, Florida 32306-4005, USA*

(Received 19 July 2013; revised manuscript received 26 August 2013; published 12 September 2013)

We used x-ray and neutron diffraction to determine the low-temperature structure of $IrTe_2$. A structural modulation was observed with a wave vector of $\boldsymbol{k} = (1/5,0,1/5)$ below $T_s \approx 285$ K, accompanied by a structural transition from a trigonal to a triclinic lattice. We also performed first-principles calculations for high-temperature and low-temperature structures, which elucidate the nature of the phase transition and the low-temperature structure. A local bonding instability associated with the Te $5p$ states is likely the origin of the structural phase transition in $IrTe_2$.

DOI: 10.1103/PhysRevB.88.115122 PACS number(s): 74.70.Xa, 74.40.Kb, 74.62.Bf

I. INTRODUCTION

The competition between a charge-density-wave (CDW) state and superconductivity is one of the most interesting phenomena in transition-metal dichalcogenides. It has been widely studied due to possible relation to high-T_c superconductivity.[1–5] Classically, CDW transitions are second-order transitions driven by Fermi surface nesting in a metal, i.e., a Kohn anomaly leading to a soft-mode instability of the high-temperature (HT) structure. A key feature of this type of transition is a coupling of the electronic structure at the Fermi energy to the structural distortion leading to strong signatures of the phase transition in transport and also in some systems an interplay between the CDW and superconductivity.

$IrTe_2$, a new member of the TX_2 family incorporating a $5d$ transition metal, exhibits superconductivity when its first-order structural transition is suppressed through doping.[6–11] Its HT structure has a trigonal symmetry with edge-sharing $IrTe_6$ octahedra forming layers stacked along the c axis with the Ir ions forming an equilateral triangular lattice [Fig. 1(a)]. The low-temperature (LT) structure was proposed to be monoclinic based on powder x-ray diffraction.[12] Accompanied with the structural transition, the resistivity shows a hump-shaped maximum and the magnetic susceptibility drops, which is similar to that of the CDW state in other TX_2 systems.[13–16]

However, recent measurements for $IrTe_2$ imply that the physics is more complicated than a simple CDW.[6–8,10,17] In particular, while optical and transport measurements do imply a strong reconstruction of the electronic structure at E_F through the transition, other measurements show that the transition is first order, which is not the generic behavior of a standard CDW. There are many possible origins for a first-order transition. One is that the mechanism is still a CDW-type related to Fermi surface nesting, but that the transition becomes first order due to coupling with strain. Another is that it is driven by local ordering, such as orbital ordering on the transition metal. Finally, a transition can be driven by chemical bonding effects.

Up to now, all the reported studies used a proposed LT structure model from powder x-ray diffraction.[12] Given that electron diffraction revealed the existence of superlattice peaks,[6] which principally also can be from the structure, the LT structure is probably more complicated than the proposed model. The correct LT structure of $IrTe_2$ is essential to explore the origin of the structural transition and explain its relationship with the superconductivity induced by doping.

In this work, we report the LT structure of $IrTe_2$ determined by using both single crystal neutron, single crystal x-ray, and powder x-ray diffraction. A modulated LT structure was solved and is distinctly different from the widely used structure model,[12] where the superstructure was not observed. We also performed first-principles calculations for the HT and LT structures, which elucidate the nature of the phase transition and the LT structure.

II. EXPERIMENTAL AND CALCULATIONAL DETAILS

Single crystals of $IrTe_2$ were grown using self-flux methods as reported.[10] The polycrystalline sample was prepared by a standard solid-state reaction. Single-crystal neutron diffraction was performed at the HB-3A four-circle diffractometer at the High Flux Isotope Reactor at Oak Ridge National Laboratory. A neutron wavelength of 1.542 Å was used from a bent perfect Si-220 monochromator.[18] Single-crystal x-ray diffraction was performed using a Bruker SMART APEX CCD diffractometer with Mo $K\alpha$ radiation. To solve the LT structure, a powder sample was measured with a PANalytical X'Pert MPD diffractometer with an incident beam monochromator (Cu $K\alpha_1$) and an Oxford Phenix Cryostat. Data were collected at 50 and 300 K. The program JANA2006 was used to solve and refine the LT structure.[19] The first-principles calculations were performed within density-functional theory using the generalized gradient approximation of Perdew, Burke, and Ernzerhof (PBE).[20] We used the general potential linearized augmented plane-wave method[21] as implemented in the WIEN2K code[22] for calculations of the electronic structure and for structure

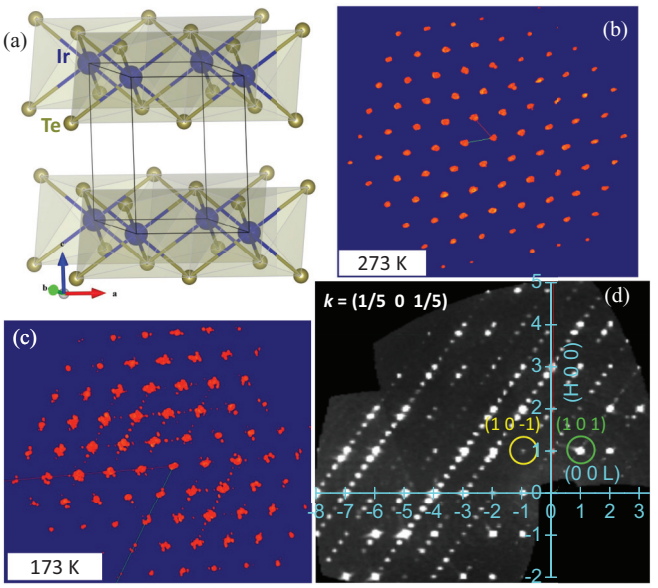

FIG. 1. (Color online) (a) The lattice structure of $IrTe_2$ in the trigonal phase at $T > T_s$; brown (blue) balls represent Te (Ir) atoms. (b) Single-crystal x-ray diffraction pattern at 273 K and (c) at 173 K. (d) (H 0 L) reciprocal plane from the pattern in (c) shows the superlattice peaks along the wave vector of (1/5, 0, 1/5). Subcell peaks (1 0 1) and (1 0 −1) are circled in green and yellow to distinguish (H 0 L) from (H 0 $-L$).

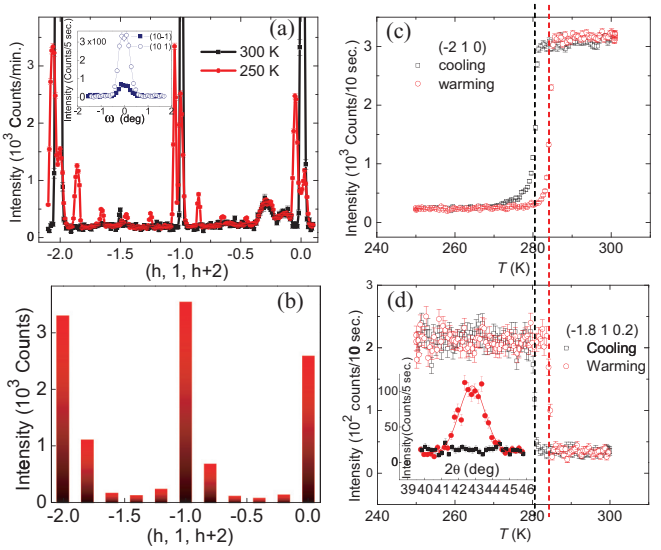

FIG. 2. (Color online) (a) $\boldsymbol{q}$ scans along (H 0 H) measured by neutron diffraction at 300 K (black solid square) and 250 K (red solid circle). The scan at 250 K shows the same wave vector of (1/5, 0, 1/5). The strong peak (1 0 1) vs the weak peak (1 0 −1) is also shown in the inset. (b) $\boldsymbol{q}$ scans along (H 0 H) from neutron diffraction calculation based on the solved LT structure [see Fig. 3(b)]. (c) and (d) Peak intensities of (−2 1 0) and (−1.8 1 0.2) with temperature warming (red open circle) and cooling (black open square) show the first-order structural transition accompanied by the superlattice structural modulation. Black and red dashed lines are guides to the eye. Inset in (d) shows the radial scan of (−1.8 1 0.2) at 300 K (black solid square) and 250 K (red solid circle).

relaxation. The VASP code[23] with projector augmented wave (PAW) pseudopotentials[24] with an energy cutoff of 300 eV was used for the phonon calculations. The phonons were obtained using a supercell approach[25] as implemented in the PHONOPY code[26] with a 4 × 4 × 3 supercell.

III. RESULTS AND DISCUSSION

The structural transition in the crystal used for x-ray diffraction occurs near $T_s \approx 264$ K during the warming process. Above T_s, trigonal $P\bar{3}m1$ symmetry was observed [Fig. 1(b)] by x rays. Below T_s, at $T = 173$ K, superlattice peaks appear and the subcell peaks split into more than four overlapped peaks [Fig. 1(c)], which makes it difficult to determine the LT lattice and to extract the peak intensity for each $\boldsymbol{q}$. By making a reciprocal plane cut, the superlattice peaks with a wave vector of (1/5, 0, 1/5) were observed [see Fig. 1(d)]. The reflections (1 0 −1) and (1 0 1) have the same $\boldsymbol{q}$ length but different intensities, which are marked in the plot and were used to determine the wave vector of (1/5, 0, 1/5). Note, the wave vector of (1/5 0 -1/5), reported by electron diffraction,[6] is equivalent to (1/5, 0, 1/5) by using different Te coordinates.

To determine the lattice parameters of the LT structure and also confirm the structural origin of the superlattice peaks, we selected a crystal with a size of 2.1 × 1.6 × 0.24 mm for the single-crystal neutron diffraction. The $\boldsymbol{q}$ scans along (H 0 H) at 300 and 250 K are plotted in Fig. 2(a), the superlattice peaks occur below T_s with the same wave vector of (1/5, 0, 1/5), which indicates that the superlattice peaks found by electron diffraction studies[6] and our x-ray diffraction are mainly caused by the structural modulation. The inset to Fig. 2(a) shows the reflections of (1 0 1) and (1 0 −1) to confirm that the reciprocal lattice is indexed in the same way as that used for the x-ray data. The structural transition was tracked by both the subcell peak (−2 1 0) and the superlattice peak (−1.8 1 0.2). The superlattice peaks occur together with the structural transition. Comparing with the crystal measured by x rays, a higher transition temperature occurs at $T_s = 285$ K during the warming process [Figs. 2(c) and 2(d)]. Since the structure refinements above T_s show the same trigonal structure, the higher T_s is likely to be associated with the residual stress caused by a faster cooling rate during the sample synthesis. Both crystals should have the same LT structure since they show almost the same diffraction pattern below T_s. The hysteresis with warming and cooling confirms that the structural transition is first-order. Below T_s, by analyzing the Bragg peaks measured in the single-crystal neutron diffraction, we obtained the trial lattice parameters of the LT structure, and they were used for indexing the powder-diffraction pattern. Due to complicated twinning (more than four domains) in the single crystal below T_s, the structure factors have not been successfully extracted.

Since the powder x-ray diffraction is insensitive to twinning, we collected data from a powder sample above and below T_s. At 300 K, the powder pattern was collected in an hour and the refinement shows that the sample has trigonal symmetry, as in the above measurements. The lattice parameters are $a = 3.9293(1)$ Å and $c = 5.3981(1)$ Å. The Appendix contains the refined powder pattern and detailed structural information. A

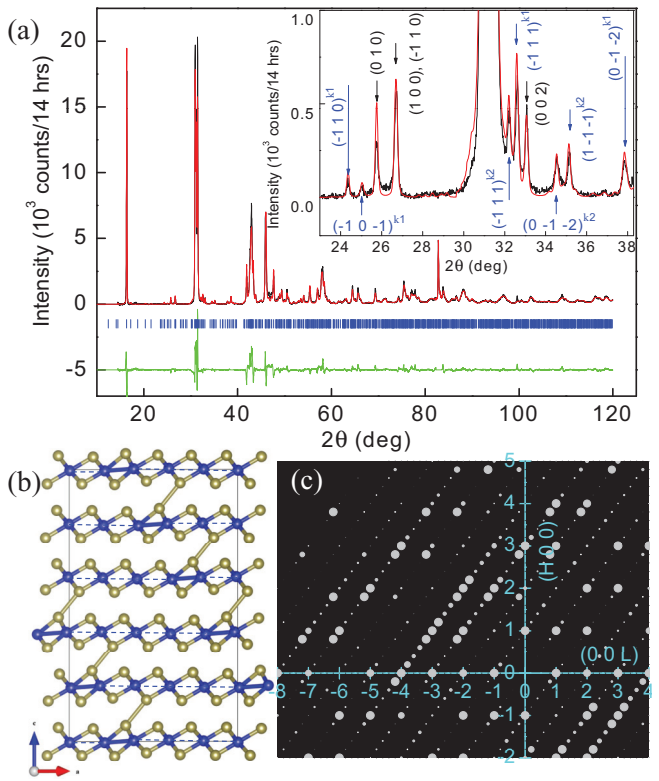

FIG. 3. (Color online) (a) Refined powder x-ray patterns at 50 K by the program JANA2006. Black and red patterns are observed and calculated, respectively. The difference is plotted in green. Blue lines mark the Bragg peak positions. The inset shows a specific data region (2θ in 22°–38°) highlighting the subcell and satellite Bragg peaks, indicated by black and blue arrows, respectively. (b) The LT superstructure. Brown (blue) balls represent Te (Ir) atoms. Ir-Te bonds are shown in brown-blue bicolor lines. The shortest Te-Te atomic distance appears in between layers, shown by brown lines, indicating the enhanced interlayer Te-Te bonding. Ir-Ir "bonds" are shown by the blue lines, solid ones represent the shortened "bond" distances, and the others are for elongated ones. (c) (H 0 L) reciprocal plane of the calculated x-ray pattern based on the LT structure.

high-quality powder diffraction pattern below T_s was measured at 50 K for 14 h. The refined pattern is shown in Fig. 3(a). With the lattice parameters and the wave vector obtained from single-crystal diffraction, we were able to index the pattern; index labels are shown in the inset. In addition to the subcell Bragg peaks, the first-order satellite Bragg peaks [$k_1 = (1/5, 0, 1/5)$] and the second-order satellite Bragg peaks [$k_2 = (2/5, 0, 2/5)$] are both indicated. The program JANA2006 was used to solve and refine the commensurately modulated LT structure in $(3 + 1)$-dimensional space.[19] The R factors of the refinement are $R = 0.036$ (for the total), $R_0 = 0.034$ (for the subcell peaks only), $R_1 = 0.037$ (for the first-order satellite peaks), and $R_2 = 0.039$ (for the second-order satellite peaks), respectively. The goodness of the refinement is also shown by the difference of the observed and calculated pattern in Fig. 3(a). With the refined superstructure [Fig. 3(b)], we calculated the single-crystal neutron and x-ray diffraction patterns. The $\boldsymbol{q}$ scan along (H 0 H) by neutrons and the [H 0 L] reciprocal plane cut by x rays are plotted in Figs. 2(b) and 3(c), respectively. They reproduce well the observed patterns in Figs. 2(a) and 1(d). The LT structure has a triclinic lattice in $P1$ symmetry, and its superstructure lattice parameters are refined as $a_s = 19.063(3)$ Å, $b_s = 3.9545(5)$ Å, $c_s = 27.089(3)$ Å, $\alpha_s = 88.74(2)°$, $\beta_s = 90.49(2)°$, and $\gamma_s = 118.99(2)°$. The volume of the subcell unit below T_s is significantly smaller than the one above T_s by 1.2%, which explains the pressure effects in our earlier work.[11] Pressure favors the phase with a smaller cell volume, and therefore the structural transition temperature was increased by applying pressure. The widely used monoclinic LT structure model[12] has a similar cell volume to that of the HT structure, which cannot explain the pressure experiment. Also in the solved LT structure [Fig. 3(b)], one Ir-Ir "bond" out of five and a part of interlayer Te-Te bonds are shortened, which is distinctly different from the previously proposed structure and is important for understanding the true origin of the structural transition in $IrTe_2$.

With the above-solved structures, we performed first-principles calculations for the electronic structure and structure relaxation. We converged basis sets consisting of standard linearized augmented plane-wave (LAPW) functions up to a cutoff $RK_{\max} = 9$, where $K_{\max}$ is the plane-wave sector cutoff and R is the minimum LAPW sphere radius; the sphere radii were 2.25 Bohr for Ir and 2.50 Bohr for Te. Additionally, local orbitals were added for the Ir $5p$ and Te $4d$ semicore states.[27]

The band structure for the HT trigonal phase, including spin orbit, is shown in Fig. 4. It is similar to the previous report of Fang and co-workers.[10] As may be seen, several bands cross the Fermi energy, E_F. The corresponding electronic density of states and Ir d projection onto the LAPW sphere is shown in Fig. 4. An examination of the projections of the density of states (DOS) reveals that the bands are of hybridized Ir $5d$–Te $5p$ character over most of the valence-band region shown. Particularly strong hybridization was noted early on by Jobic and co-workers.[28]

The consequence of this strong hybridization is that there is no clear separation into nominally Ir derived and nominally Te derived bands. Therefore, one should not apply nominal ionic models, e.g., $Ir^{4+}Te_2^{2-}$, to understand this compound. This is reflected in the bond valence sums (see the Appendix),[29] which deviate strongly from the nominal ionic values of 4 and 2 for Ir and Te, respectively. This is not surprising both because as a $5d$ element Ir may be expected to show substantial hybridization with ligands due to its extended d shell, and also because as a late transition element it has a high electronegativity of 2.20 (Pauling scale), which is comparable to and actually larger than the value of 2.1 for the metalloid element, Te. Importantly, this means that one has partially filled Te $5p$ shells in this compound, and as a result Te-Te bonding is expected to be important.

Importantly, the bands around E_F show dispersion both in the plane of the $IrTe_2$ layers and also rather strongly in the c-axis direction. This is seen in the dispersions along the Γ-A line and also in the differences in dispersions along the A-L-H-A path from those along Γ-M-K-Γ. This reflects bonding between the Te atoms in neighboring layers. This bonding is also clearly reflected in the crystal structure. The nearest Te-Te distance is 3.49 Å, and is across the gap between adjacent $IrTe_2$ sheets. The nearest distance between Te atoms across a sheet is 3.55 Å, while that within a hexagonal Te layer on one side of a

$IrTe_2$ sheet is 3.93 Å, i.e., much longer. In any case, such three dimensionality of the electronic structure is not favorable for nesting and distinguishes the present compound from CDW materials such as $NbSe_2$ where some bands crossing E_F are three-dimensional but the bands comprising the nested Fermi surface are rather two-dimensional.[30,31]

We also did electronic structure calculations for the LT experimental structure and for a calculated structure. The calculated structure was obtained by taking the LT lattice parameters from experiment and fully relaxing the atomic coordinates to minimize the total energy. The relaxation was done using the LAPW method in a scalar relativistic approximation. This structure differed from the experimental structure in that it has less variation of the Ir bond valence sums than the experimental structure. However, as seen in the calculated electronic density of states (Fig. 5), the results for this structure and the experimental structure are very similar, although the energy for the calculated structure is lower by 94 meV per formula unit as compared to the experimental structure.

The DOS shows a strong reduction at E_F, from 1.82 eV^{-1} per formula unit for the HT structure to 1.00 eV^{-1} per formula unit for the experimental LT structure and 1.02 eV^{-1} per formula unit for the calculated structure. This sizable

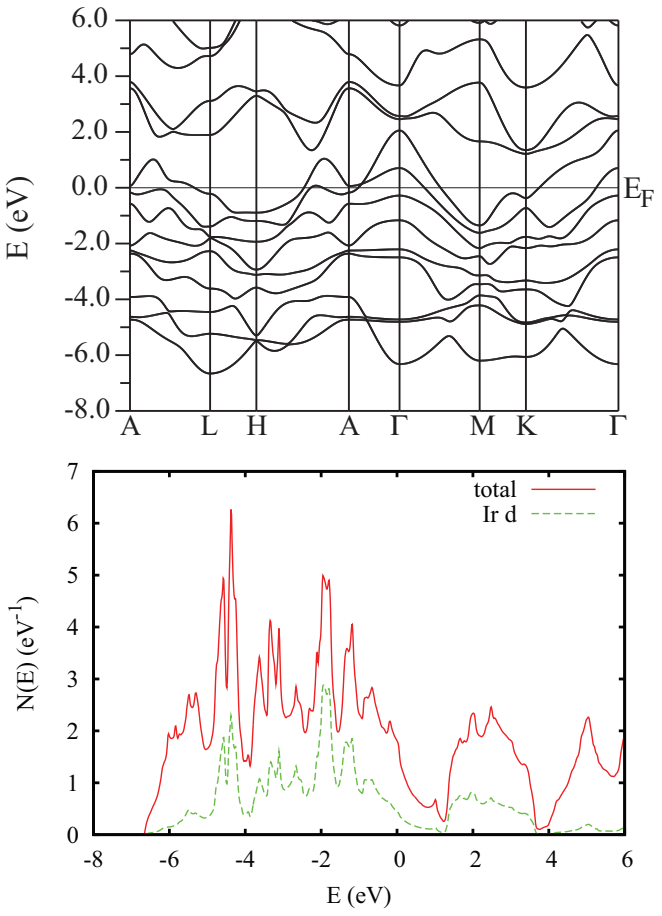

FIG. 4. (Color online) Calculated band structure of $IrTe_2$ HT trigonal structure. Spin orbit is included. The lower panel shows the electronic density of states for the HT phase along with the Ir *d* projection onto the LAPW sphere.

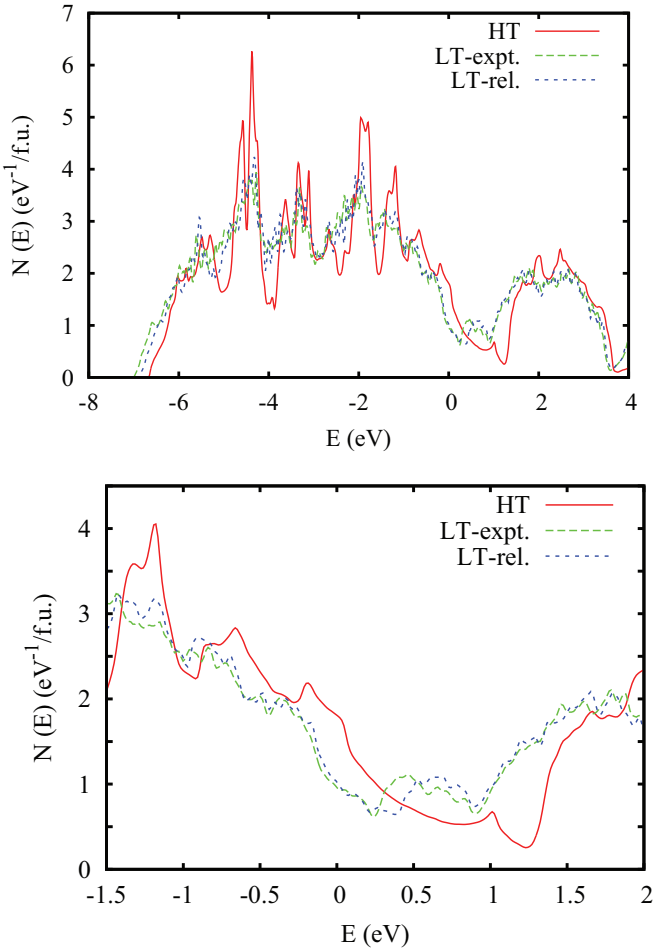

FIG. 5. (Color online) Calculated electronic density of states for $IrTe_2$ in the HT structure and the LT structure. The lower panel is an enlargement near E_F.

change is consistent with the large changes in transport and optical properties as observed[10] through the phase transition, which is generically what is expected for a CDW. However, one observes that the DOS is reconstructed by the structural distortion over a large energy range ~ -1.0 to $+1.5$ eV (we give energies relative to E_F). This is in contrast to a standard

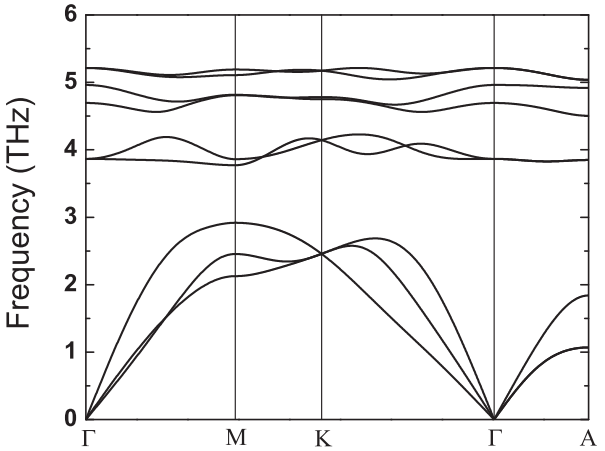

FIG. 6. Calculated phonon dispersions of $IrTe_2$ in the HT trigonal structure.

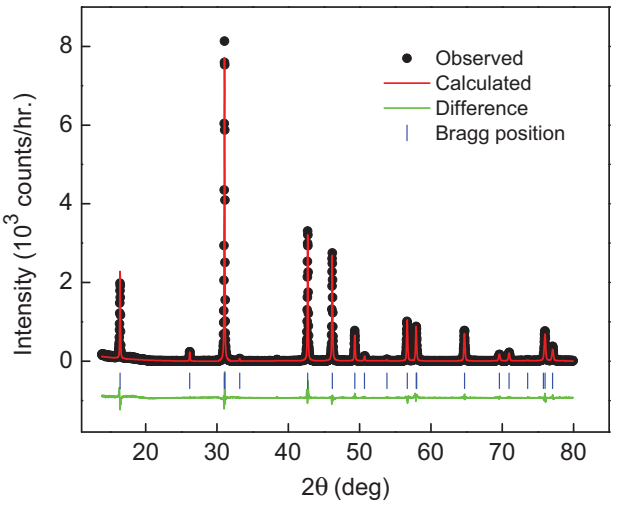

FIG. 7. (Color online) The refined powder x-ray pattern at 300 K. Black and red patterns are observed and calculated, respectively. The difference is plotted in green. Blue lines mark the Bragg peak positions.

CDW, where the reconstruction is over a range of a few kT_N, even in a strong-coupling case. Furthermore, the change in the DOS is not well described as a gapping around E_F with a shift of spectral weight to energies just above or below the gap as in a CDW. Instead, there is a downward shift of all the occupied valence states and a shift of a rather broad pseudogap in the DOS from the region around ∼1 eV to the region around ∼0 eV. Furthermore, we do not find a redistribution of the Ir-Te hybridization. Specifically, the DOS in the gapped region retains a similar mixture of Ir $5d$ and Te $5p$ character to the undistorted region. This shows that the distortion is associated mainly with the Te $5p$ states, rather than Ir-Te bonding. The large energy range over which the electronic structure is reconstructed is consistent with recent optical measurements.[10] It will be of interest to perform additional spectroscopic measurements, e.g., by scanning probes and or photoemission, to compare in detail with the rearrangements of the electronic structure predicted based on the present crystal structure determinations. This is characteristic of a rearrangement of the local bonding, and not a CDW.

The calculated phonon dispersions of $IrTe_2$ in the HT trigonal phase are shown in Fig. 6. As may be seen, no unstable branches nor any unusual dips would suggest Kohn anomalies.

TABLE I. Refined HT structural parameters of $IrTe_2$ from the powder x-ray data at 300 K, space group $P\bar{3}m1$. The lattice parameters are $a = 3.9295(1)$ Å and $c = 5.3984(1)$ Å. $Rf = 0.038$, $Rp = 0.129$, and $\chi^2 = 3.66$.

Atom	x	y	z	B_{iso}
Ir	0	0	0	0.7(1)
Te	1/3	2/3	0.7465(7)	0.4(1)

This contradicts what would be expected for a material that undergoes a CDW.

IV. CONCLUSIONS

In conclusion, the LT structure of $IrTe_2$ was solved by using x-ray and neutron diffraction. The superlattice peaks were observed with the wave vector of (1/5, 0, 1/5) and the associated structural modulation was identified. The first-principles calculations based on the LT structure revealed that the first-order structural transition in $IrTe_2$ is in a class that strongly couples to the electronic structure around E_F, but is not related to a Fermi surface instability as in a CDW. Instead it is associated with a local bonding instability associated with the Te $5p$ states. This is consistent with the conclusions of Fang and co-workers.[10]

ACKNOWLEDGMENTS

This work was supported by the US Department of Energy, Office of Basic Energy Sciences. H.C. and B.C.C. are supported by the Scientific User Facilities Division. X.C., J.Y., M.A.M., D.J.S., and D.M. are supported by the Materials Sciences and Engineering Division. R.C. is supported by the Division of Chemical Sciences, Geosciences, and Biosciences. H.Y. would thank the China Scholarship Council for financial assistance.

APPENDIX: STRUCTURE

The refined powder x-ray pattern of $IrTe_2$ at 300 K and the HT and LT structure information are presented (see Fig. 7 and Tables I– III).

The average bond valence sums for the LT structures are $v_{Ir} = 7.16$ and $v_{Te} = 4.68$ for the experimental structure, and $v_{Ir} = 6.91$ and $v_{Te} = 4.55$ for the calculated structure. The bond valence sums for the HT structure are $v_{Ir} = 7.15$ and $v_{Te} = 4.61$.

TABLE II. Refined LT structure of $IrTe_2$ from the powder x-ray data at 50 K is presented in space group $P1$, lattice parameters, $a_s = 19.063(3)$ Å, $b_s = 3.9545(5)$ Å, $c_s = 27.089(3)$ Å, $\alpha_s = 88.74(2)^\circ$, $\beta_s = 90.49(2)^\circ$, and $\gamma_s = 118.99(2)^\circ$. $R0 = 0.034$, $R1 = 0.037$, $R2 = 0.039$, $Rf = 0.036$, $Rp = 0.125$, $\chi^2 = 3.85$. Ir atomic coordinates are in fractions of the lattice parameters, in space group $P1$ with the first Ir atom chosen to be at (0,0,0) for the experimental (Expt.) and calculated (Calc.) structures. The bond valence sums, v, are given.

	Expt.				Calc.			
Atom	x	y	z	v	x	y	z	v
Ir	0.0000	0.0000	0.0000	7.60	0.0000	0.0000	0.0000	6.80
Ir	0.2095	0.9791	0.0016	7.74	0.2098	0.9818	0.9983	7.00
Ir	0.4154	0.9568	0.9984	6.40	0.4146	0.9571	0.9960	6.97
Ir	0.8000	0.0000	0.2000	7.60	0.8000	0.0000	0.2000	6.81
Ir	0.0095	0.9791	0.2016	7.74	0.0098	0.9818	0.1983	7.00

TABLE II. (*Continued*.)

	Expt.				Calc.			
Atom	*x*	*y*	*z*	*v*	*x*	*y*	*z*	*v*
Ir	0.2154	0.9568	0.1984	6.40	0.2146	0.9571	0.1960	6.97
Ir	0.6275	0.9124	0.1924	7.26	0.6313	0.9199	0.1925	6.80
Ir	0.4201	0.9341	0.1936	6.79	0.4199	0.9349	0.1939	6.98
Ir	0.8095	0.9791	0.4016	7.74	0.8098	0.9818	0.3983	7.00
Ir	0.0154	0.9568	0.3984	6.40	0.0146	0.9571	0.3960	6.97
Ir	0.6000	0.0000	0.4000	7.60	0.6000	0.0000	0.4000	6.81
Ir	0.2201	0.9341	0.3936	6.79	0.2199	0.9349	0.3939	6.98
Ir	0.4275	0.9124	0.3924	7.26	0.4312	0.9199	0.3925	6.80
Ir	0.8154	0.9568	0.5984	6.40	0.8146	0.9571	0.5960	6.97
Ir	0.4000	0.0000	0.6000	7.60	0.4000	0.0000	0.6000	6.81
Ir	0.6095	0.9791	0.6016	7.74	0.6098	0.9818	0.5983	7.00
Ir	0.0201	0.9341	0.5936	6.79	0.0199	0.9349	0.5939	6.98
Ir	0.2275	0.9124	0.5924	7.26	0.2312	0.9199	0.5924	6.80
Ir	0.2000	0.0000	0.8000	7.60	0.2000	1.0000	0.8000	6.80
Ir	0.4095	0.9791	0.8016	7.74	0.4098	0.9818	0.7983	7.00
Ir	0.6154	0.9568	0.7984	6.40	0.6146	0.9571	0.7960	6.97
Ir	0.8201	0.9341	0.7936	6.79	0.8199	0.9349	0.7939	6.98
Ir	0.0275	0.9124	0.7924	7.26	0.0313	0.9199	0.7925	6.80
Ir	0.6201	0.9341	0.9936	6.79	0.6199	0.9349	0.9939	6.98
Ir	0.8275	0.9124	0.9924	7.26	0.8313	0.9199	0.9925	6.80

TABLE III. Te atomic coordinates are in fractions of the lattice parameters, in space group $P1$ with the first Ir atom chosen to be at (0,0,0) for the experimental (Expt.) and calculated (Calc.) structures. The bond valence sums are denoted by v.

	Expt.				Calc.			
Atom	*x*	*y*	*z*	*v*	*x*	*y*	*z*	*v*
Te	0.6868	0.5661	0.1422	5.44	0.6846	0.5615	0.1375	4.83
Te	0.8759	0.6823	0.1547	5.06	0.8733	0.6731	0.1495	4.50
Te	0.0761	0.6432	0.1481	4.34	0.0777	0.6470	0.1477	4.66
Te	0.2860	0.6279	0.1454	4.41	0.2822	0.6229	0.1444	4.44
Te	0.4923	0.6097	0.1450	4.74	0.4895	0.6053	0.1436	4.34
Te	0.6759	0.6823	0.3547	5.06	0.6733	0.6731	0.3494	4.50
Te	0.8761	0.6432	0.3481	4.34	0.8777	0.6470	0.3477	4.66
Te	0.0860	0.6279	0.3454	4.41	0.0822	0.6229	0.3444	4.44
Te	0.2923	0.6097	0.3450	4.74	0.2895	0.6053	0.3436	4.34
Te	0.4868	0.5661	0.3422	5.44	0.4846	0.5615	0.3375	4.83
Te	0.6761	0.6432	0.5481	4.34	0.6777	0.6471	0.5477	4.66
Te	0.8860	0.6279	0.5454	4.41	0.8822	0.6229	0.5444	4.44
Te	0.0923	0.6097	0.5450	4.74	0.0895	0.6053	0.5436	4.34
Te	0.2868	0.5661	0.5422	5.44	0.2846	0.5615	0.5375	4.83
Te	0.4759	0.6823	0.5547	5.06	0.4733	0.6731	0.5494	4.50
Te	0.6860	0.6279	0.7454	4.41	0.6822	0.6230	0.7444	4.44
Te	0.8923	0.6097	0.7450	4.74	0.8895	0.6053	0.7436	4.34
Te	0.0868	0.5661	0.7422	5.44	0.0846	0.5615	0.7375	4.83
Te	0.2759	0.6823	0.7547	5.06	0.2733	0.6731	0.7494	4.50
Te	0.4761	0.6432	0.7481	4.34	0.4777	0.6470	0.7476	4.66
Te	0.6923	0.6097	0.9450	4.74	0.6895	0.6053	0.9436	4.34
Te	0.8868	0.5661	0.9422	5.44	0.8846	0.5615	0.9375	4.83
Te	0.0759	0.6823	0.9547	5.06	0.0733	0.6731	0.9494	4.50
Te	0.2761	0.6432	0.9481	4.34	0.2777	0.6470	0.9477	4.66
Te	0.4860	0.6279	0.9454	4.41	0.4822	0.6230	0.9444	4.44
Te	0.7591	0.2443	0.0433	4.45	0.7570	0.2461	0.0423	4.49
Te	0.9527	0.3678	0.0552	4.78	0.9466	0.3604	0.0550	4.83
Te	0.1431	0.3130	0.0499	4.69	0.1412	0.3132	0.0490	4.37

TABLE III. (*Continued*.)

	Expt.				Calc.			
Atom	*x*	*y*	*z*	*v*	*x*	*y*	*z*	*v*
Te	0.3425	0.2806	0.0487	4.67	0.3475	0.2919	0.0479	4.43
Te	0.5521	0.2677	0.0478	4.26	0.5518	0.2690	0.0444	4.62
Te	0.7527	0.3678	0.2552	4.78	0.7466	0.3604	0.2550	4.83
Te	0.9431	0.3130	0.2499	4.69	0.9412	0.3132	0.2490	4.37
Te	0.1425	0.2806	0.2487	4.67	0.1475	0.2919	0.2479	4.43
Te	0.3521	0.2677	0.2478	4.26	0.3518	0.2690	0.2444	4.62
Te	0.5591	0.2443	0.2433	4.45	0.5570	0.2461	0.2424	4.49
Te	0.7431	0.3130	0.4499	4.69	0.7412	0.3133	0.4490	4.37
Te	0.9425	0.2806	0.4487	4.67	0.9475	0.2920	0.4478	4.43
Te	0.1521	0.2677	0.4478	4.26	0.1518	0.2690	0.4444	4.62
Te	0.3591	0.2443	0.4433	4.45	0.3570	0.2461	0.4423	4.49
Te	0.5527	0.3678	0.4552	4.78	0.5466	0.3604	0.4550	4.83
Te	0.7425	0.2806	0.6487	4.67	0.7475	0.2920	0.6478	4.43
Te	0.9521	0.2677	0.6478	4.26	0.9518	0.2690	0.6444	4.62
Te	0.1591	0.2443	0.6433	4.45	0.1570	0.2461	0.6423	4.49
Te	0.3527	0.3678	0.6552	4.78	0.3466	0.3604	0.6550	4.83
Te	0.5431	0.3130	0.6499	4.69	0.5412	0.3133	0.6490	4.37
Te	0.7521	0.2677	0.8478	4.26	0.7518	0.2690	0.8444	4.62
Te	0.9591	0.2443	0.8433	4.45	0.9570	0.2461	0.8423	4.49
Te	0.1527	0.3678	0.8552	4.78	0.1466	0.3604	0.8550	4.83
Te	0.3431	0.3130	0.8499	4.69	0.3412	0.3132	0.8490	4.37
Te	0.5425	0.2806	0.8487	4.67	0.5475	0.2919	0.8478	4.43

*caoh@ornl.gov

[1] R. L. Withers and J. A. Wilson, J. Phys. C **19**, 4809 (1986).

[2] J. A. Wilson and A. D. Yoffe, Adv. Phys. **28**, 193 (1969).

[3] J. A. Wilson, F. J. DiSalvo, and S. Mahajan, Adv. Phys. **24**, 117 (1975).

[4] K. Rossnagel, J. Phys.: Condens. Matter **23**, 213001 (2011).

[5] E. Morosan, H. W. Zandbergen, B. S. Dennis, J. W. G. Bos, Y. Onose, T. Klimczuk, A. P. Ramirez, N. P. Ong, and R. J. Cava, Nat. Phys. **2**, 544 (2006).

[6] J. J. Yang, Y. J. Choi, Y. S. Oh, A. Hogan, Y. Horibe, K. Kim, B. I. Min, and S-W. Cheong, Phys. Rev. Lett. **108**, 116402 (2012).

[7] S. Pyon, K. Kudo, and M. Nohara, J. Phys. Soc. Jpn. **81**, 053701 (2012).

[8] D. Ootsuki, Y. Wakisaka, S. Pyon, K. Kudo, M. Nohara, M. Arita, H. Anzai, H. Namatame, M. Taniguchi, N. L. Saini, and T. Mizokawa, Phys. Rev. B **86**, 014519 (2012).

[9] M. Kamitani, M. S. Bahramy, R. Arita, S. Seki, T. Arima, Y. Tokura, and S. Ishiwata, Phys. Rev. B **87**, 180501(R) (2013).

[10] A. F. Fang, G. Xu, T. Dong, P. Zheng, and N. L. Wang, Nat. Sci. Rep. **3**, 1153 (2013).

[11] A. Kiswandhi, J. S. Brooks, H. B. Cao, J. Q. Yan, D. Mandrus, Z. Jiang, and H. D. Zhou, Phys. Rev. B **87**, 121107(R) (2013).

[12] N. Matsumoto, K. Taniguchi, R. Endoh, H. Takano, and S. Nagata, J. Low Temp. Phys. **117**, 1129 (1999).

[13] C. Hejny and M. I. McMahon, Phys. Rev. Lett. **91**, 215502 (2003).

[14] M. I. McMahon, C. Hejny, J. S. Loveday, L. F. Lundegaard, and M. Hanfland, Phys. Rev. B **70**, 054101 (2004).

[15] C. Hejny, L. F. Lundegaard, S. Falconi, M. I. McMahon, and M. Hanfland, Phys. Rev. B **71**, 020101(R) (2005).

[16] I. Loa, M. I. McMahon, and A. Bosak, Phys. Rev. Lett. **102**, 035501 (2009).

[17] K. Mizuno, K. Magishi, Y. Shinonome, T. Saito, K. Koyama, N. Matsumoto, and S. Nagata, Physica B **312-313**, 818 (2002).

[18] B. C. Chakoumakos, H. Cao, F. Ye, A. D. Stoica, M. Popovici, M. Sundaram, W. Zhou, J. S. Hicks, G. W. Lynn, and R. A. Riedel, J. Appl. Crystallogr. **44**, 655 (2011).

[19] V. Petricek, M. Dusek, and L. Palatinus, JANA2006 (Institute of Physics, Praha, Czech Republic, 2006).

[20] J. P. Perdew, K. Burke, and M. Ernzerhof, Phys. Rev. Lett. **77**, 3865 (1996).

[21] D. J. Singh and L. Nordstrom, *Planewaves Pseudopotentials and the LAPW Method*, 2nd ed. (Springer, Berlin, 2006).

[22] P. Blaha, K. Schwarz, G. Madsen, D. Kvasnicka, and J. Luitz, *WIEN2k, An Augmented Plane Wave + Local Orbitals Program for Calculating Crystal Properties* (Tech. Univ. Wien, Austria, 2001).

[23] G. Kresse and J. Furthmuller, Phys. Rev. B **54**, 11169 (1996).

[24] G. Kresse and D. Joubert, Phys. Rev. B **59**, 1758 (1999).

[25] K. Parlinski, Z-.Q. Li, and Y. Kawazoe, Phys. Rev. Lett. **78**, 4063 (1997).

[26] A. Togo, F. Oba, and I. Tanaka, Phys. Rev. B **78**, 134106 (2008).

[27] D. Singh, Phys. Rev. B **43**, 6388 (1991).

[28] S. Jobic, P. Deniard, R. Brec, J. Rouxel, A. Jouanneaux, and A. N. Fitch, Z. Anorg. Allg. Chem. **598**, 199 (1991).

[29] I. D. Brown and D. Altermatt, Acta Cryst. B **41**, 244 (1985).

[30] M. D. Johannes, I. I. Mazin, and C. A. Howells, Phys. Rev. B **73**, 205102 (2006).

[31] D. S. Inosov, V. B. Zabolotnyy, D. V. Evtushinsky, A. A. Kordyuk, B. Buchner, R. Follath, H. Berger, and S. V. Borisenko, New J. Phys. **10**, 125027 (2008).